Science of the Total Environment 482–483 (2014) 174–183

Contents lists available at ScienceDirect

Science of the Total Environment

journal homepage: www.elsevier.com/locate/scitotenv

Optical characterization of black water blooms in eutrophic waters

Hongtao Duan [a,*], Ronghua Ma [a], Steven Arthur Loiselle [b], Qiushi Shen [a], Hongbin Yin [a], Yuchao Zhang [a]

[a] State Key Laboratory of Lake Science and Environment, Nanjing Institute of Geography and Limnology, Chinese Academy of Sciences, Nanjing 210008, China
[b] Dipartimento Farmaco Chimico Tecnologico, CSGI, University of Siena, 53100 Siena, Italy

HIGHLIGHTS

- Black water blooms have led to major problems in eutrophic waters and water supplies.
- The bio-optical properties of black water blooms were compared to typical lake waters.
- Low reflectance was associated with high CDOM absorption and low SPIM backscattering.
- The black water blooms are favored by macrophyte die back during periods of low wind speed.

ARTICLE INFO

Article history:
Received 2 December 2013
Received in revised form 17 February 2014
Accepted 25 February 2014
Available online xxxx

Keywords:
Black water masses
Biogeochemical cycles
Aquatic vegetation
Dissolved organic carbon

ABSTRACT

In the summer of 2007, blooms of "black" water in Lake Taihu entered into the potable water supply of Wuxi City and left more than 1 million people without water. Attempts to monitor these black water blooms have not been successful due to their irregular nature. In May 2012, two black water blooms were observed in one of the lake's eutrophic bays. The bio-optical analyses of these blooms show that they were dominated by higher concentrations of dissolved organic matter and lower backscattering coefficients with respect to the surrounding lake conditions. We show the contribution of each optically active component to the perceived radiance and demonstrate that elevated absorption due to dissolved organic matter and phytoplankton combined with reduced backscattering led to the perception of these water areas as "black", while the true color was dark green. The present analysis indicates that formation of black water blooms is favored during springtime conditions in the macrophyte dominated areas of the lake's hypereutrophic bays.

1. Introduction

Water color was first used to define water masses by the Swiss limnologist Francoise-Alphonse Forel in the late 1800s in a nonquantitative classification approach (Arnone et al., 2004). The color of water is directly related to the concentrations and optical properties of the dissolved and suspended matter in the water column and their impact on the upward flux of scattered radiance perceived by the observer (IOCCG, 2000, 2008). The most important of these are usually phytoplankton, non-algal particulates, chromophoric dissolved organic matter (CDOM) and the water itself (Morel, 1988). In general, CDOM increases absorption in the short visible wavelengths, reducing upwelling radiance and increasing overall attenuation (Battin, 1998; Berthon and Zibordi, 2010; Zhao et al., 2013). Phytoplankton can also lead to significant changes in water color, with both increase attenuation and increased scattered radiance (Dierssen et al., 2006).

The color of water perceived by the human eye can be numerically described by the color matching functions defined by the Commission Internationale de l'Ĕclairage (CIE), which transpose radiometric measurements onto a colorimetric coordinate system (Dierssen et al., 2006; Watanabe et al., 2011). Differences in perceived color imply differences in the underwater optical conditions. However, the underlying relationship between apparent optical properties (AOPs) and water color is still poorly understood in most coastal and inland waters due to the complexity of optical conditions, where absorption and scattering of phytoplankton pigments, non-algal particulates, and CDOM may spectrally overlap (IOCCG, 2000).

Lake Taihu, the third largest freshwater lake in China, provides fundamental services to a large surrounding population, even though it is one of the most severely polluted freshwater reservoirs in China (Duan et al., 2009; Hu et al., 2010). Agricultural activities are the major source of non-point pollution while the growing urban communities within the basin and the limited treatment of urban wastewater represent the most important point pollution source (Qin et al., 2007). In the summer of 2007, water quality problems, initially associated with algal blooms, left more than 1 million people in the city of Wuxi without drinking water (Guo, 2007). Further studies indicated that the apparent cause was the intrusion of a black water bloom of unknown origin into the main water intake of the city (Yang et al., 2008). While

* Corresponding author.
E-mail addresses: htduan@niglas.ac.cn, htduan@gmail.com (H. Duan).

http://dx.doi.org/10.1016/j.scitotenv.2014.02.113
0048-9697/

black water blooms had been previously reported (Lu and Ma, 2010), it was only after the 2007 occurrence that academic and government authorities began to treat black water blooms as an environmental priority.

Black water blooms, black water agglomerates, black spots or dead zones have been characterized as hypoxic and malodorous areas of freshwater and marine ecosystems (Diaz and Rosenberg, 2008; Feng et al., 2014; Pucciarelli et al., 2008). They often have elevated sulfide concentrations, principally metal sulfides and hydrogen sulfide (Duval and Ludlam, 2001; Lu and Ma, 2010; Stahl, 1979) associated with the presence of sulfate-reducing bacteria and degrading organic matter from algal blooms or sediment (Feng et al., 2014; He et al., 2013). They present significant threats to drinking water safety. Black blooms have occurred in many inland lakes and continental seas, such as Lake Kasumigaura (Japan) (Sugiura and Nakano, 2000), Lower Mystic Lake (USA) (Duval and Ludlam, 2001), Lake Garda (Italy) (Pucciarelli et al., 2008), Florida Keys (USA) (Hu et al., 2004), Baltic (Europe) (Berthon and Zibordi, 2010), and East China Sea (Bai et al., 2009).

In May 2012, black water blooms were observed during regular *in-situ* algal bloom monitoring activities. Field measurements were made immediately to characterize the bio-optical properties of two of these black water masses. These data provided an opportunity to explore the possible causes of their occurrence and potential methods for their monitoring. To the best of our knowledge, this is the first study to optically address the occurrence of black water blooms in waters destined for human consumption.

2. Materials and methods

2.1. Fieldwork

Water samples and optical data were collected at 12 stations from three areas of Gonghu Bay, Lake Taihu on 17th May, 2012 (Fig. 1). Two areas (Zones 1 and 2) were identified as "black" water areas with samples taken from an area of typical lake water (Zone 3) in the center. At each station, remote sensing reflectance (R_{rs}) was measured with an ASD hand-held spectrometer, following the NASA Ocean Optics protocols (Mueller and Fargion, 2003). The viewing angle of the measurement was ~40° from nadir, and the relative azimuth angle to the sun was ~135°. Data from several stations (Nos. 1–3, 5–6) were removed due to low signal to noise ratio. Water samples were collected just below the surface with a standard 2-liter polyethylene water-sampler

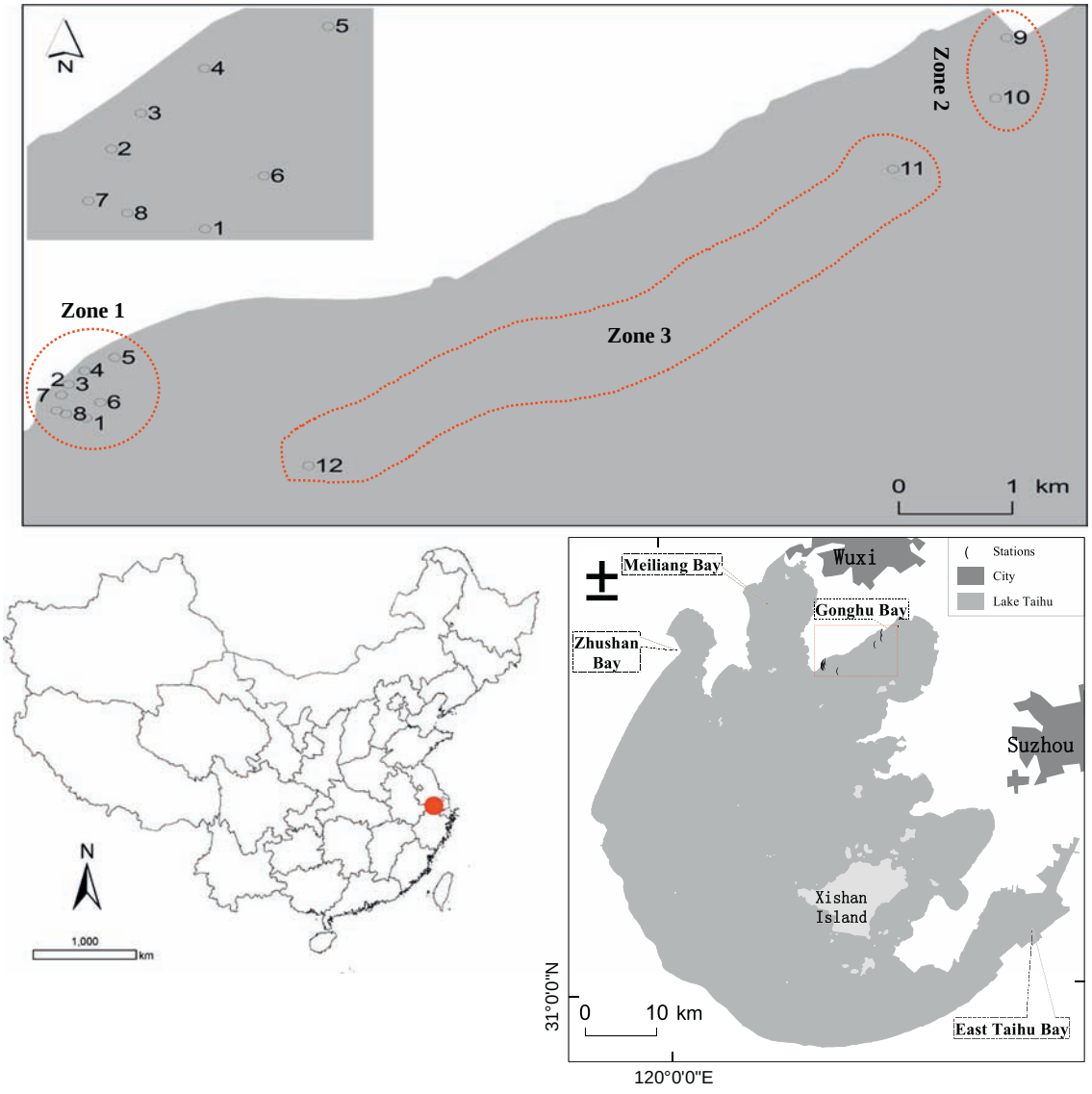

Fig. 1. Sampling sites in Gonghu Bay, Lake Taihu (China) near the potable water source for Wuxi City. Black water masses were present in Zone 1 (stations 1–8) and Zone 2 (stations 9–10) with typical lake waters characterizing Zone 3 (stations 11–12).

immediately after R_{rs} measurement. The samples were stored with ice bags in the dark for less than 4 h before chemical and optical measurements were made in the laboratory.

2.2. Concentrations of optically active components

Chla concentrations were extracted using 90% ethanol and measured with a UV2401 spectrophotometer (Strickland and Parsons, 1972). Suspended particulate matter (SPM) concentrations were determined gravimetrically from samples collected on pre-combusted and pre-weighed GF/F filters with a diameter of 47 mm, dried at 95 °C over night. SPM was differentiated by gravimetric analysis into suspended particulate inorganic matter (SPIM) and suspended particulate organic matter (SPOM) after treating the filters at 550 °C for 3 h (Ma et al., 2006). Dissolved organic matter (DOC) concentrations were determined after filtration through pre-combusted 47 mm GF/F filters, with a Shimadzu TOC-5000A analyzer (Chen et al., 2004).

2.3. Optical characteristics

Spectral absorption coefficients of total particulate matter ($a_p(\lambda)$), phytoplankton pigments ($a_{ph}(\lambda)$), and non-phytoplankton particulate matter ($a_d(\lambda)$) were determined using the quantitative filter technique with 47-mm GF/F filters and a Shimadzu UV2401 spectrophotometer (Mitchell, 1990; Mueller and Fargion, 2003; Yentsch, 1962). CDOM absorption ($a_g(\lambda)$) was determined following filtration (Millipore filter with 0.22-μm pore size) using a spectrophotometer and distilled water as the reference. The exponential absorption slope ($S_{400-700}$) of the CDOM spectra was calculated by a nonlinear fitting of absorption from 400 to 700 nm as (Bricaud et al., 1981):

$$a_{400-700}(\lambda) = a_{400-700}(\lambda_0)\exp[-S_{400-700}(\lambda_0-\lambda)] \quad (1)$$

where λ_0 is the reference wavelength (443 nm). The distribution of the absorption spectral slope (S_λ) was calculated using a non-linear fitting method based on least squares regression from 220 nm to 400 nm at a 20 nm wavelength interval (Loiselle et al., 2009).

A HydroScat-6 backscattering sensor was used to measure total backscattering coefficient (b_b) at six wavelengths of 420, 442, 470, 510, 590 and 700 nm following the standard protocol (Maffione and Dana, 1997). The particulate backscatter coefficient (b_{bp}) was calculated by subtracting the backscattering coefficient of pure water (b_{bw}) and expressed as (Ma et al., 2009; Sathyendranath et al., 2001; Wu et al., 2011):

$$b_{bp}(\lambda) = b_{bp}(\lambda_0)\left(\frac{\lambda_0}{\lambda}\right)^n \quad (2)$$

where n is the wavelength dependence of particulate scattering, λ_0 is the reference wavelength (590 nm) corresponding to the mounted band in HS-6 (IOCCG, 2006).

2.4. Visually perceived water color

Water color will depend on the quantity and spectral quality of upwelling light at the water surface, R_{rs}, which is governed by the ratio of backscattering (b_b) to absorption (a) (Gordon and Morel, 1983):

$$R_{rs}(\lambda) = \frac{ft}{Qn^2}\frac{b_b(\lambda)}{a(\lambda)+b_b(\lambda)} \quad (3)$$

where $a(\lambda)$ can be separated into the spectral absorption of each optically active component of the water column (a_{ph}, a_d, a_g) and pure water (a_w); while b_b is the measurement of total backscattering. The terms f and Q are parameters that depend on local optical conditions and wavelength, and their ratio, f/Q varies less than f and Q individually (Morel and Gentili, 1993) while still being influenced by solar angle and the ratio of scattering to absorption in Case 2 waters (Loisel and Morel, 2001); t/n^2 (t is the water-to-air diffuse transmittance and n is the refractive index of water) is approximately equal to 0.54 (Austin, 1974; Clark, 1981). A lake specific spectral correction factor $\gamma(\lambda)[=0.54f/Q]$ was determined from measurements of each optically active component and the measured R_{rs}:

$$\text{measured } R_{rs}(\lambda) = \gamma(\lambda)\frac{b_b(\lambda)}{b_b(\lambda)+a_g(\lambda)+a_{ph}(\lambda)+a_d(\lambda)+a_w(\lambda)}. \quad (4)$$

The CIE color components (X, Y, and Z) were calculated as the product of the water-leaving radiance (L_w) and the three tristimulus functions integrated over the visible spectrum (400–700 nm), and then transformed into RGB primaries using a matrix transform based on the chromaticity coordinates and reference white of a standard computer monitor (Dierssen et al., 2006):

$$\begin{bmatrix} R \\ G \\ B \end{bmatrix} = \begin{bmatrix} 3.240479 & -1.537150 & -0.498535 \\ -0.969256 & 1.875992 & 0.041556 \\ 0.055648 & -0.204043 & 1.057311 \end{bmatrix} \times \begin{bmatrix} X \\ Y \\ Z \end{bmatrix}. \quad (5)$$

The resulting RGB values ranged from 0 to 1 and represented the fractional amount of each primary needed to display a particular color on a computer monitor. Values calculated to be less than 0 were set to 0 and values greater than 1 were set to 1 (Dierssen et al., 2006). The human observer was assumed to look directly down at the water surface with no sun glint or bright sky reflection.

3. Results

The two black water areas (Zones 1 and 2, Fig. 1) had an extension of less than 1 km^2. Both areas were surrounded by aquatic vegetation. Zone 1 had emergent macrophytes at its borders (*Phragmites australis*), while Zone 2 had submerged macrophytes (*Potamogeton crispus*). The control area, Zone 3, had typical lake conditions for Gonghu Bay and without nearby macrophyte stands.

An analysis of the optical and chemical properties of the two black water areas showed significant differences in DOC and backscattering coefficients compared to non-black waters of the lake (Zone 3) (t-test, $p < 0.05$). DOC concentrations were highest in Zones 1 and 2 (Table 1). Chla concentrations were highest in Zone 2 and lowest in Zone 3. The percentage of organic particulate matter (SPOM) in the total particular matter was highest in Zones 1 and 2 (38% higher) with respect to Zone 3, while SPIM and its ratio to SPM were highest in Zone 3. SPM was strongly correlated with SPIM ($r = 0.85$, $p < 0.01$), while Chla was well correlated with SPOM ($r = 0.82$, $p < 0.01$).

3.1. Optical characterization

The measured R_{rs} spectra showed large variations in magnitude and shape with clear differences between lake areas (Fig. 2a–c). Zone 1 R_{rs} curves were the lowest, with a relatively wide peak around 500–550 nm (<0.008 sr^{-1}). Zone 2 R_{rs} showed a peak around 550 nm (<0.014 sr^{-1}) with significant attenuation between 650 and 700 nm. Zone 3 R_{rs} curves had the highest reflectance with a peak around 550 nm (<0.035 sr^{-1}). $R_{rs}(555)/R_{rs}(412)$ increased from Zone 1 (<1.3) to Zone 2 (>2.1) to Zone 3 (>2.4). With respect to the typical lake waters of Zone 3, the waters of Zones 1 and 2 had a lower average reflectance (400–700 nm) (Fig. 2d).

CDOM absorption at 443 nm ($a_g(443)$) was two times higher in Zones 1 and 2 with respect to Zone 3 (Fig. 3a). Regression analyses between $a_g(443)$ and DOC showed significant power and linear relationships; $a_g(443) = 0.0054\text{DOC}^{2.91}$ ($R^2 = 0.77$, $p < 0.01$), and $a_g(443) = 0.34\text{DOC}-0.98$ ($R^2 = 0.68$, $p < 0.01$) (Fig. 4a). The absorption spectral slope distribution (S_λ) showed significant differences between the

Table 1
Bio-optical water quality parameters of black water blooms and typical lake waters in Lake Taihu.

	All ($n = 12$)		Zone 1 ($n = 8$)		Zone 2 ($n = 2$)		Zone 3 ($n = 2$)	
	Mean	Range	Mean	Range	Mean	Range	Mean	Range
DOC (mg L^{-1})	5.49 ± 1.11	3.53–7.02	5.95 ± 0.88	4.32–7.02	5.31 ± 0.91	4.67–5.96	3.84 ± 0.44	3.53–4.15
Chla (μg L^{-1})	21.44 ± 22. 47	3.05–78.32	13.39 ± 6.55	3.05–20.34	58.38 ± 28.20	38.44–78.32	3.88	3.88
SPM (mg L^{-1})	15.93 ± 5.83	7.80–26.20	14.15 ± 4.45	7.80–22.40	21.08 ± 3.29	18.75–23.40	17.88 ± 11.77	9.55–26.20
SPOM (mg L^{-1})	6.72 ± 3.13	3.25–12.10	6.57 ± 3.00	3.30–11.40	9.93 ± 3.08	7.75–12.10	4.13 ± 1.24	3.25–5.00
SPIM (mg L^{-1})	9.20 ± 5.34	4.50–21.20	7.58 ± 3.63	4.50–15.95	11.15 ± 6.36	6.65–15.65	13.75 ± 10.54	6.30–21.20
$a_g(443)$ (m^{-1})	0.86 ± 0.45	0.37–1.68	0.97 ± 0.50	0.38–1.68	0.90 ± 0.17	0.78–1.03	0.42 ± 0.06	0.37–0.46
S_g (nm^{-1})	0.0160 ± 0.0049	0.0096–0.0251	0.0168 ± 0.0059	0.0096–0.0251	0.0142 ± 0.0003	0.0140–0.0145	0.0143 ± 0.0002	0.0142–0.0144
$a_d(443)$ (m^{-1})	0.70 ± 0.31	0.32–1.52	0.72 ± 0.36	0.32–1.52	0.68 ± 0.21	0.53–0.83	0.60 ± 0.25	0.42–0.78
$a_{ph}(443)$ (m^{-1})	1.07 ± 0.58	0.50–2.58	0.88 ± 0.31	0.50–1.36	1.92 ± 0.93	1.26–2.58	0.95 ± 0.63	0.51–1.40
$a^*_{ph}(443)$ (m^2 mg^{-1})	0.07 ± 0.05	0.03–0.16	0.08 ± 0.05	0.04–0.16	0.03 ± 0.00	0.03–0.03	0.13	0.13
$a_p(443)$ (m^{-1})	1.76 ± 0.65	0.93–3.40	1.80 ± 0.65	1.30–3.40	2.60 ± 1.13	1.80–3.40	1.55 ± 0.88	0.93–2.17
$a_t(443)$ (m^{-1})	2.63 ± 0.86	1.31–4.43	2.57 ± 0.67	1.82–3.43	3.50 ± 1.31	2.58–4.43	1.97 ± 0.94	1.31–2.64
$b_{bp}(590)$ (m^{-1})	0.18 ± 0.09	0.11–0.42	0.13 ± 0.01	0.11–0.15	0.24 ± 0.03	0.22–0.26	0.29 ± 0.18	0.17–0.42
n (Eq. 2)	−2.16 ± 0.35	−3.00–−1.68	−2.04 ± 0.20	−2.1–−1.68	−2.05 ± 0.24	−2.22–−1.88	−2.78 ± 0.31	−3.00–−2.56

Chla: chlorophyll-a; SPM: suspended particulate matter; SPOM: suspended particulate organic matter; SPIM: suspended particulate inorganic matter; $a_g(443)$: CDOM absorption coefficient at 443 nm; S_g: the spectral slope of CDOM absorption; $a_d(443)$: detritus absorption coefficient at 443 nm; $a_{ph}(443)$: phytoplankton absorption coefficient at 443 nm; $a_t(443)$: total absorption coefficient at 443 nm; $b_{bp}(590)$: the particulate backscatter coefficient at 590 nm. Black water blooms were present in Zone 1 (stations 1–8) and Zone 2 (stations 9–10); typical lake waters were present in Zone 3 (stations 11–12).

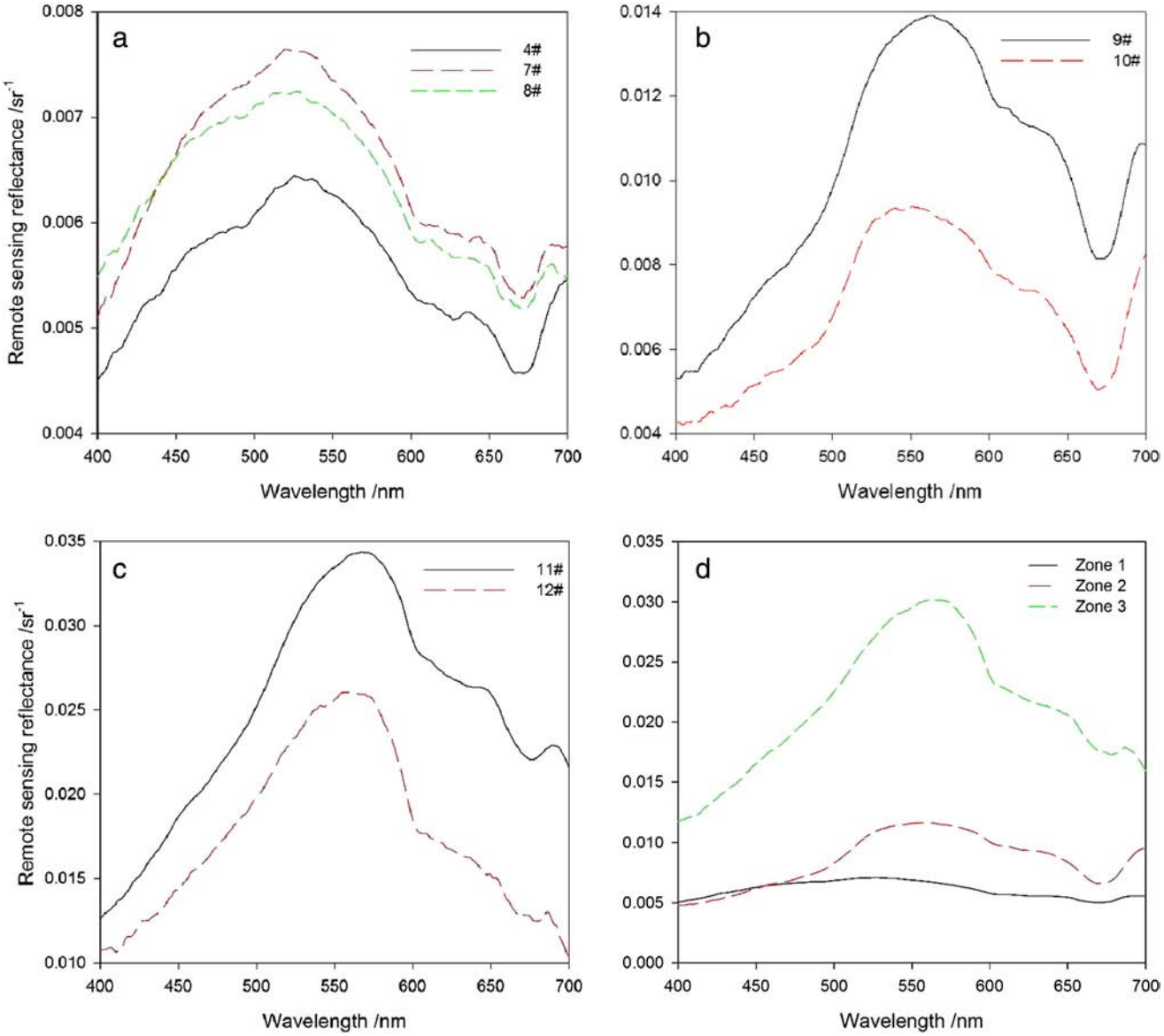

Fig. 2. Reflectance spectra (sr^{-1}) for surface waters from stations in: (a) Zone 1; (b) Zone 2; (c) Zone 3; and (d) average reflectance spectra of Zone 1, Zone 2 and Zone 3.

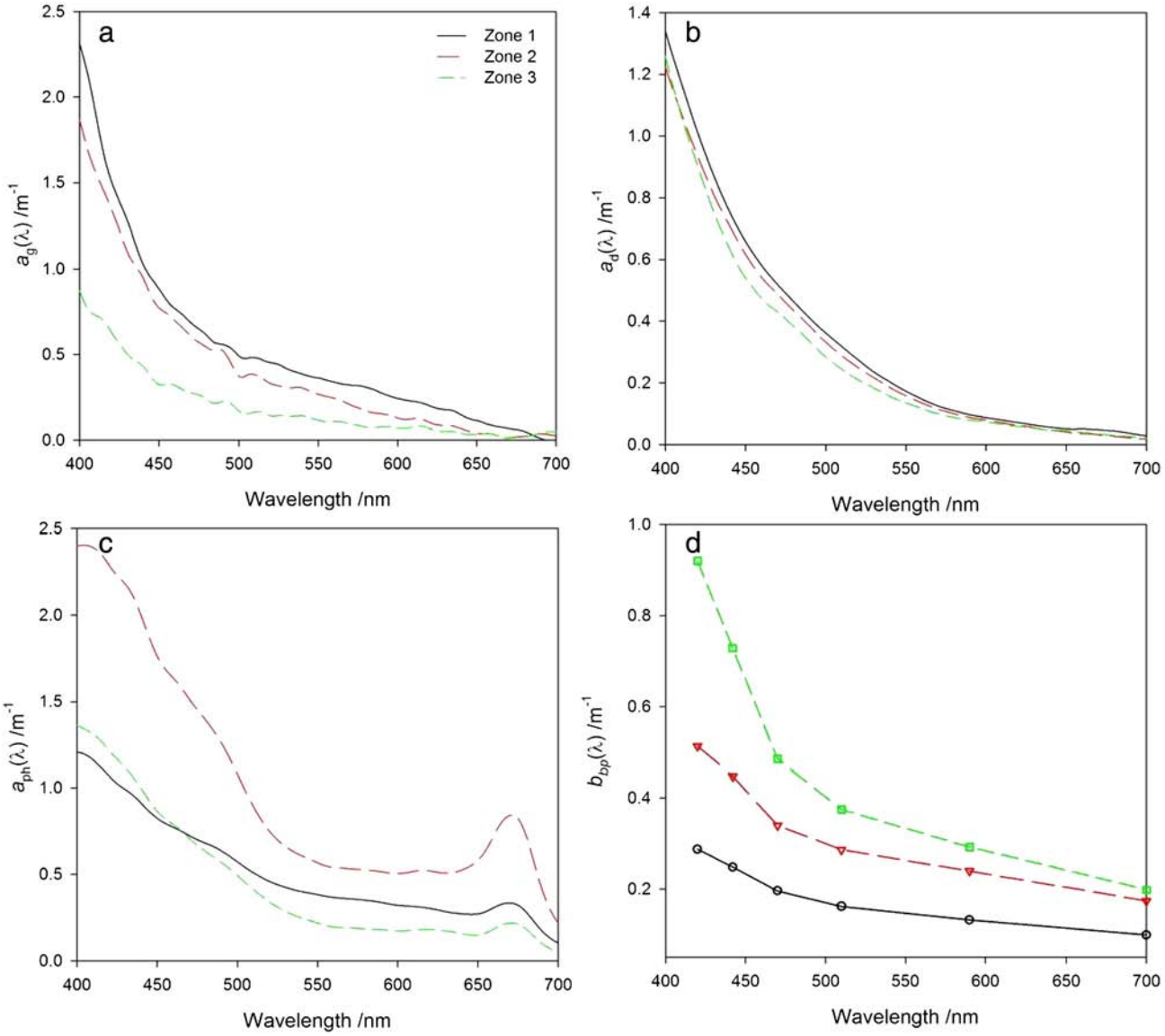

Fig. 3. The average absorption spectra from 400 to 700 nm for each zone related to: (a) chromophoric dissolved organic matter ($a_g(\lambda)$), (b) detritus ($a_d(\lambda)$), (c) phytoplankton pigments ($a_{ph}(\lambda)$), and (d) the coefficient for particulate backscattering ($b_{bp}(\lambda)$).

black water zones and Zone 3 in most wavelengths (t-test, $p < 0.05$) with a maximum difference at 298 nm. Differences between Zones 1 and 2 were evident in a limited wavelength range (262–264 nm). The relationship between $S_{400-700}$ and $a_g(443)$ indicated a similarity between CDOM sources in Zones 1 and 2 (Fig. 4b).

The particulate backscatter coefficients were significantly higher in Zone 3, in all wavelengths. $b_{bp}(590)$ was lowest in Zone 1, 80% higher in Zone 2, and more than double in Zone 3 (Fig. 3d). $b_{bp}(590)$ values were significantly correlated with SPM ($R^2 = 0.52$, $p < 0.01$) and SPIM ($R^2 = 0.61$, $p < 0.01$), but not correlated to SPOM ($p > 0.50$), indicating the relative importance of inorganic detritus in backscattering (Le et al., 2013; Tzortziou et al., 2007). It should be noted that the $b_{bp}(\lambda)$ spectra in Zone 1 (stations 1–8) varied over a narrow range, compared to more significant variation between stations in Zones 2 and 3. The $b_{bp}(\lambda)$ spectra of station 11 had the highest value which coincided with elevated concentrations of SPM and SPIM.

The $a_d(\lambda)$ values were highest in Zones 1 and 2, while $a_{ph}(\lambda)$ showed the expected bimodal distribution (Fig. 3b, c). The specific-absorption coefficient for phytoplankton pigment at 443 nm ($a_{ph}^*(443)$) was between 0.03 and 0.16 m^2 mg^{-1}. Previous studies have associated this variation with package effects (Bricaud et al., 2004; Naik et al., 2013). $a_p(\lambda)$ showed the greatest variation of any of the component spectra (Fig. 3d) with the value $a_p(443)$ ranging from 0.93 to 3.40 m^{-1}. This variable was significantly correlated with Chla ($r = 0.86$, $p < 0.01$) and SPOM ($r = 0.57$, $p < 0.01$), but poorly with SPM and SPIM ($r < 0.4$, $p > 0.10$).

3.2. Optical closure

The relationship between the inherent optical properties (IOPs) of the components of the water column and apparent optical properties (AOPs) was explored using *in situ* measured IOPs as inputs to $R_{rs}(\lambda)$ (Eq. 4) and $\gamma(\lambda) = 1$. The overall agreement between the variation in the estimated $R_{rs}(\lambda)$ values and measured $R_{rs}(\lambda)$ values was elevated ($r > 0.88$, $p < 0.005$). It should be noted that multiple sources of uncertainty may contribute to an imperfect agreement between estimated $R_{rs}(\lambda)$ and measured $R_{rs}(\lambda)$, including potential errors in the measurements of $b_{bp}(\lambda)$, $a(\lambda)$, and $R_{rs}(\lambda)$. Moreover, the simple radiative transfer expression (Eq. 4) and correction factor do not consider variations in ambient conditions between stations, related to surface roughness, cloud cover, solar angle, and vertical effects within the upper waters (O'Donnell et al., 2010). The spectral correction factor for the lake, $\gamma(\lambda)$, was then determined (Eq. 4) and found to spectrally vary within

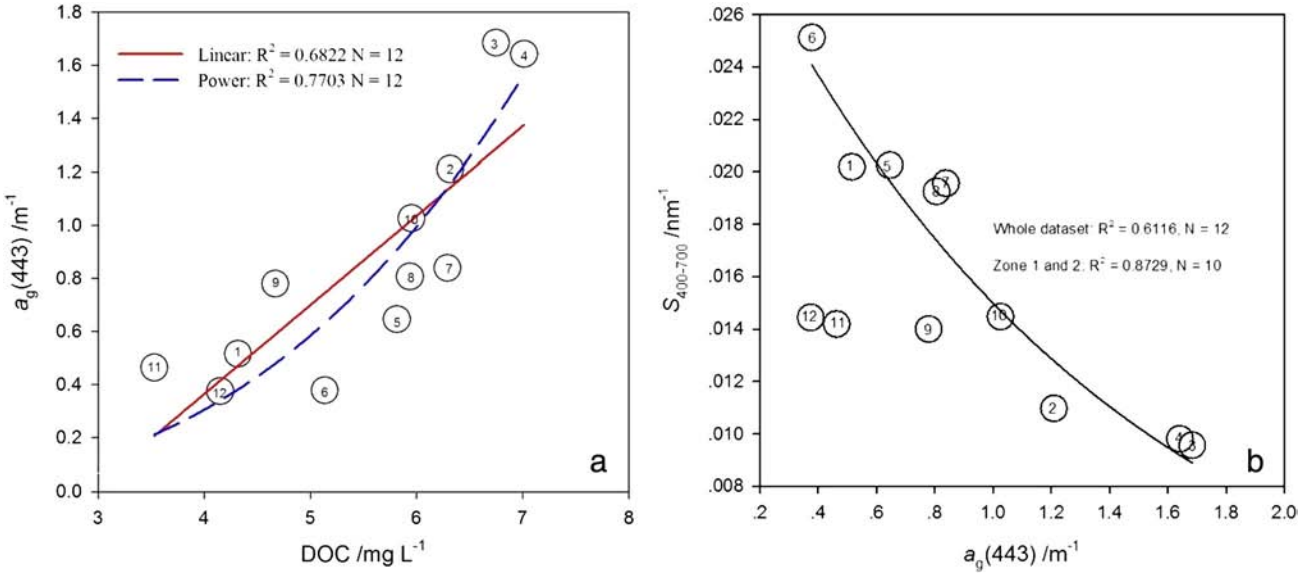

Fig. 4. The relationships between (a) CDOM absorption at 443 nm (a_g(443)) and dissolved organic carbon (DOC); (b) between CDOM absorption at 443 nm (a_g(443)) and absorption spectral slope ($S_{400-700}$). The solid line represents the power model on all data. Open circles represent station numbers.

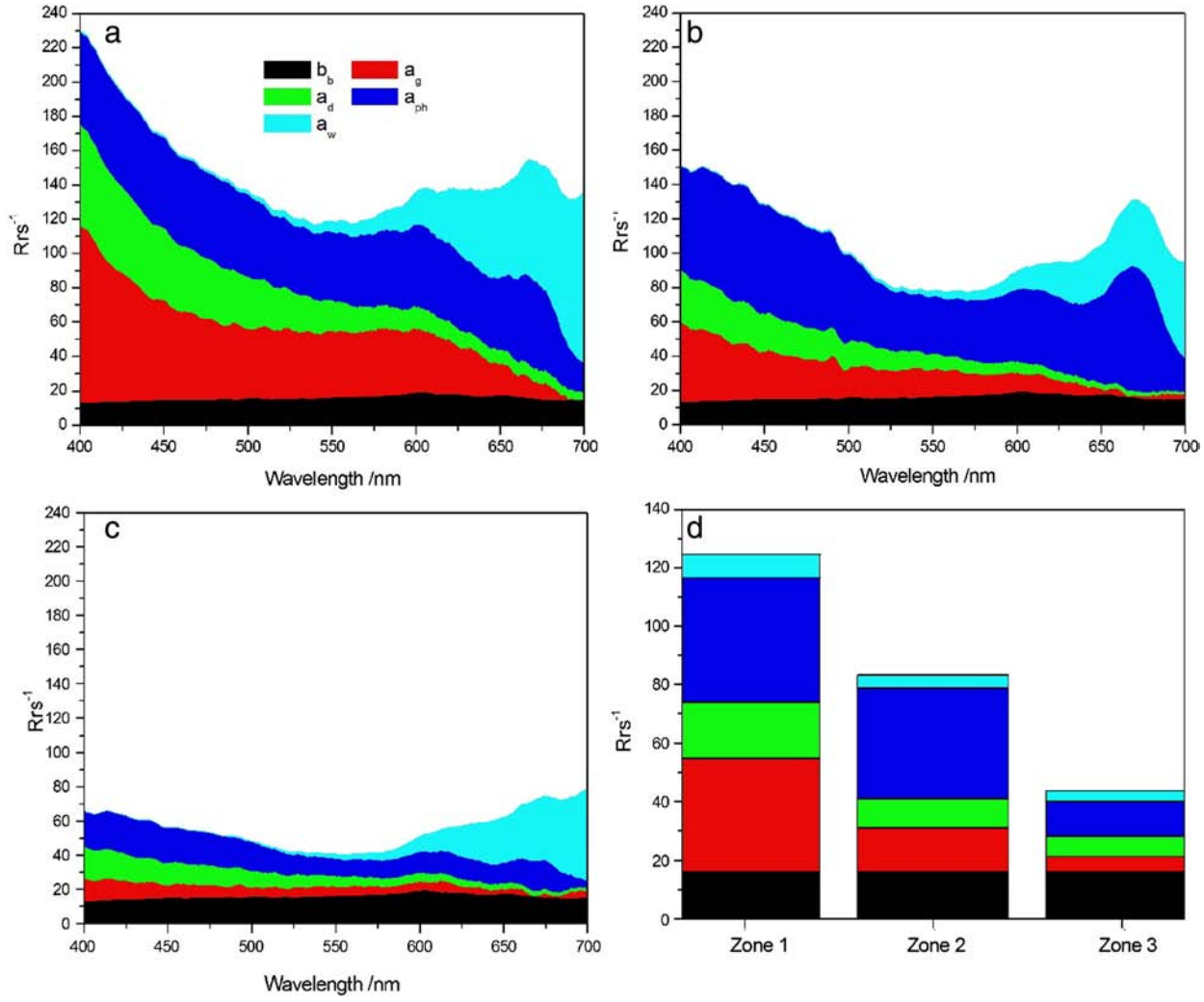

Fig. 5. Contributions of individual optical components to R_{rs}^{-1} in: (a) Zone 1; (b) Zone 2; and (c) Zone 3. (d) Integrated R_{rs}^{-1} over 500–600 nm considering the photonic luminous efficiency of the human eye. Note that R_{rs}^{-1} is defined by Eq. (6).

values (0.05–0.08) expected for model Case 2 waters (Loisel and Morel, 2001).

The contribution of individual optically active components was explored utilizing the inverse of the radiative transfer expression, R_{rs}^{-1} (Eq. 4) and the spectral correction factor for the lake, $\gamma(\lambda)$:

$$R_{rs^{-1}}(\lambda) = \frac{1}{R_{rs}(\lambda)} = \gamma(\lambda)^{-1}\frac{b_b(\lambda) + a_g(\lambda) + a_{ph}(\lambda) + a_d(\lambda) + a_w(\lambda)}{b_b(\lambda)} \quad (6)$$

By separating the individual contributions of each term, it was possible to identify the optical components that dominated R_{rs}^{-1} and therefore the reduction in reflectance. The total R_{rs}^{-1} at each λ (Eq. 6) provided the expected relationship between zones, with the largest R_{rs}^{-1} occurring in Zones 1 and 2 with respect to Zone 3 in all wavelengths (Fig. 5a–c).

Considering that the photonic luminous efficiency of the human eye is maxima between 500 and 600 nm, the individual contributions to R_{rs}^{-1} were integrated over this waveband to identify the relative difference in total perceived color of each area. Zone 1 had an ${R_{rs}}^{-1}{}_{500-600}$ that was 3 times that of Zone 3 and 28% higher than Zone 2 (Fig. 5d). Given these conditions in the R_{rs} and R_{rs}^{-1}, Zone 1 would appear the darkest to the human eye, followed by Zone 2.

The water surface color, transposed using the CIE color matching functions from *in situ* measured water-leaving radiance, indicates that the color of the lake water from Zone 1 should appear dark olive drab green and the Zone 2 should appear olive-green, while Zone 3 would appear sea-green (Fig. 6a).

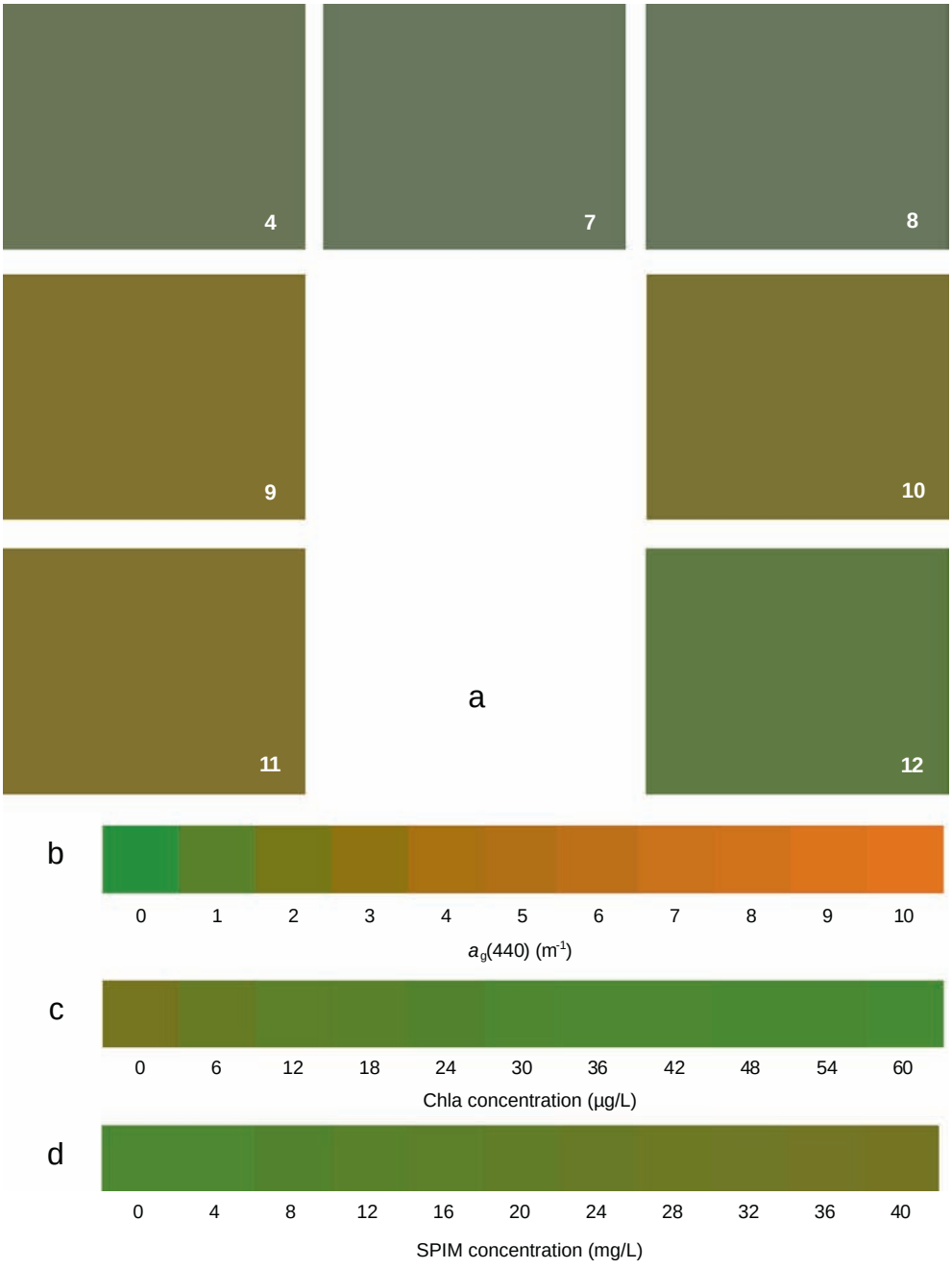

Fig. 6. (a) Modeled surface color based on water-leaving radiance using the CIE color matching functions. Color of the water surface as a function of increasing concentrations of: (b) $a_g(440)$ between 0 and 10 m^{-1}; (c) Chla between 0 and 60 µg L^{-1}; and (d) SPIM between 0 and 40 mg L^{-1}.

4. Discussion

4.1. Why do black waters appear black?

The color perceived by the human visual system depends largely on the total radiance incident upon each type of cone and the comparative response (*i.e.*, contrast) between the three cone classes (red, green, and blue) (Dierssen et al., 2006). The water surface color, transposed using the CIE color matching functions from *in situ* measured water-leaving radiance, indicates that the color of the upwelling radiance observed in the black water zones was not black, but different shades of green (Fig. 6a). Although black is generally defined as the visual impression experienced when no visible light reaches the eye, water masses look "black" when there is a significant reduction in the light reflected back to the observer with respect to the surrounding surfaces. Zones 1 and 2 appeared "black" due to the high contrast with the surrounding lake waters with a relatively higher R_{rs} (Fig. 3). This contrast allows for the determination of an edge, basic for the recognition of shapes (McCollough, 1965).

The contribution of each optically active component to the contrast between different waters (Eq. 6) indicated that the elevated R_{rs}^{-1} of Zone 1 was strongly controlled by CDOM (a_g) below 500 nm and by Chla absorption (a_{ph}) between 500 nm and 600 nm (Fig. 5a). Above 600 nm, water related absorption dominated R_{rs}^{-1}. Zone 2 high R_{rs}^{-1} was strongly controlled by both Chla absorption and CDOM below 500 nm (Fig. 5b). Above 500 nm, R_{rs}^{-1} was dominated by Chla related absorption. Zone 3 had the lowest R_{rs}^{-1}, which was dominated by backscattering and Chla absorption below 500 nm (Fig. 5c). Above 500 nm, backscattering was the largest contributor to R_{rs}^{-1} until 600 nm, after which water related absorption became the largest contributor.

The integrated contributions of each optically active component, considering the photonic luminous efficiency of the human eye confirmed that Zone 1 had the highest R_{rs}^{-1}, dominated by a_{ph} (34%) and CDOM (31%). Zone 2 was dominated by a_{ph} (45%). From these measurements, the higher absorption by CDOM in Zone 1 and phytoplankton biomass in Zone 2 were the cause of the perceived darkness with respect to normal lake waters (Zone 3), where backscattering dominated (37%) radiative transfer. The relative spectral qualities of each section agreed with the estimated color water-leaving radiance using the CIE matching functions (Fig. 6b–d).

4.2. Why do black waters occur?

Water color is directly related to the optically properties of its dissolved and particulate components. These components are, in turn, influenced by local biogeochemical processes, including leaf litter decomposition (IOCCG, 2000, 2008). In most water bodies, aquatic plants follow an annual cycle of growth, reproduction and senescence. However, surveys in Lake Taihu have found that aquatic macrophytes often undergo a spring die-back and a subsequent release of residual plant matter into surrounding lake areas, including Zones 1 and 2 (Shen et al., 2014). According to Diaz & Rosenberg (2008), black blooms require a large quantity of degrading organic matter, from either autochthonous sources (phytoplankton, aquatic macrophytes) or allochthonous organic matter. With the combined occurrence of phytoplankton blooms and macrophyte die-back, the possibility of hypoxia and black blooms is enhanced in the spring.

Under natural conditions, macrophyte die-back should not occur in the spring. However, local fisherman often use steel fishing nets to harvest benthic fauna which cause extensive damage to areas of submerged plants. While the use of this equipment is prohibited in the spring, our consultations with the local environmental protection department and fisherman indicate that steel fishing nets continue to be widely used.

4.2.1. High CDOM

CDOM, the optically active fraction of DOC, may originate from terrestrially derived materials from plant degradation (allochthonous), as well as from microbial sources within the water body (autochthonous) (Clark et al., 2008; Loiselle et al., 2012; Zhang et al., 2009). The overall increase in CDOM in Zones 1 and 2, with respect to the open lake waters suggests that there is a net production of CDOM in these areas. This is confirmed in the relationship between spectral slope and absorption, indicating that the CDOM in Zones 1 and 2 may have origins that are different than those of the CDOM in Zone 3 (Fig. 4b). This would suggest that the large stands of *P. australis* and *P. crispus* may contribute CDOM to nearby waters (Barber et al., 2001; Stabenau et al., 2004; Tzortziou et al., 2008). Leaf litter decomposition typically occurs in three, often simultaneous phases: (1) leaching of soluble components, (2) microbial oxidation of refractory components, and (3) physical and biological fragmentation. The initial rapid weight loss observed has been attributed to leaching of soluble organic compounds (Chimney and Pietro, 2006; Davis et al., 2003; Valiela et al., 1985), which contribute to increasing the concentrations of DOC and CDOM (Wang et al., 2007). The second and third phases include the microbially mediated breakdown of labile organic material and refractory structural components, which make up the bulk of leaf mass (Davis et al., 2003; Valiela et al., 1985). The 'labile' fraction of organic matter, such as glucose, is rapidly decomposed within a few days while the 'refractory' fraction is decomposed more slowly (Mostofa et al., 2013). These latter stages of decay can result in a significant accumulation of N and P (Pascoal and Cassio, 2004). "Black water" generally occurs in extreme anaerobic environments, accompanied often by strong septic and marshy odors (Yang et al., 2008), which were observed in Zones 1 and 2 (Shen et al., 2014). During anoxic conditions, a significant amount of protein-like and humic-like DOM may accumulate due to slower bacterial utilization (Wang et al., 2007). The largest differences in the distribution of the absorption spectral slope (S_λ) occurred at 298 nm, with the lowest in Zone 1 (0.018) and highest in Zone 3 (0.026) and indicating differences in the molecular characteristics of the residual CDOM present (Loiselle et al., 2009).

4.2.2. High Chla

The release of DOC from macrophytes or phytoplankton has been linked to changes in phytoplankton biomass and productivity (Clark et al., 2008; Hu et al., 2004; Zhang et al., 2009). Macrophyte die off, in particular *Potamogeton* spp. has been associated with increased nutrient and chlorophyll-a concentrations in shallow lakes (Sayer et al., 2010). The significant release and accumulation of nutrients during the last stage of leaf decomposition will stimulate algal growth, either phytoplanktonic or epiphytic (Pedersen and Borum, 1996; Twilley et al., 1985). Jansson et al. (1996) showed that the increased bacterial production in colored lakes may supply phosphorus to potential autotrophic organisms.

4.2.3. High SPOM and Low SPIM

Local hydrodynamics will have a strong effect on the concentration of suspended particulates, both plankton and detritus related. The presence of aquatic macrophytes reduces wave energy, flow velocities and sediment resuspension (Madsen et al., 2001; Squires et al., 2002). Reduced turbidity and increase light availability create a positive feedback to promote further growth and reproduction of macrophytes. With reduced flow velocities, macrophyte beds are often areas of sediment accumulation, as deposition is favored over resuspension (Losee and Wetzel, 1993). This is particularly important for the deposition rate of SPIM, which is higher than that of SPOM. Measurements in Lake Taihu indicted that the settling velocity of SPIM is 2.5–5.5 times higher than that of SPOM for low wind speeds (<3.5 m/s) similar to those present in the days prior to black water event (Xiang et al., 2008).

4.3. Optical monitoring of black water blooms

Regular measurements using satellite based remote optical sensors (MODIS) in Lake Taihu over the last decade indicate that the lowest R_{rs} occurs in the spring, yet satellite identified that black water blooms have not been reported (Duan et al., 2012, 2010) (Fig. 7). This suggests that the radiometric, temporal or spatial thresholds of available sensors may be insufficient to identify black water events, typically limited in size (0.01 to 2 km^2) and of short duration (in 2–3 days). One potential approach to identify these areas is may be to focus on areas of particularly high CDOM. Several algorithms have been proposed to investigate the spatial and temporal dynamics of CDOM in inland and coastal waters (Lee et al., 2002; Morel and Gentili, 2009; Shanmugam, 2011), including one for Lake Taihu (Jiang et al., 2012). With additional observations of black water blooms, a better identification of potential causes would be possible.

In situ optical (including visual) measurements in areas where macrophyte stands are present would allow for observational data with a higher temporal frequency. These measurements would be particularly useful during periods of elevated algal blooms and low wind. While the spatial, temporal and spectral resolution of remote optical sensors are insufficient to meet this challenge, the identification of macrophyte stands as potential areas for the formation of black water blooms opens up the possibility for their *in-situ* monitoring.

Conflict of interest

The authors declared that they have no conflict of interest to this work.

Acknowledgments

The authors would like to thank all participants and voluntary contributors (Guangjia Jiang, Changfeng Wang, Zeren Wang, Jiahui Huang, Xiaoyu Pang and Mengxiao Ma [Nanjing Institute of Geography and Limnology, Chinese Academy of Sciences: NIGLAS]). Thanks also for the MATLAB code that was used for determining the RGB color of a spectrum developed by Heidi M. Dierssen [University of Connecticut]. Data are provided by the Scientific Data Sharing Platform for Lake and Watershed (SDSPLW), NIGLAS and the Dragon 3 program (10561). Financial support was provided by the National Project on Water Pollution Control and Management (2012ZX07103-005), the National Natural Science Foundation of China (41171271, 41171273 and 41101316), and the 135-Program of NIGLAS (NIGLAS2012135014 and NIGLAS2012135010).

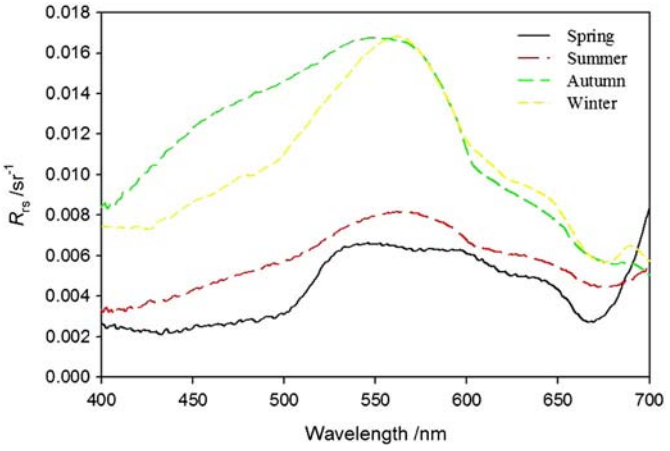

Fig. 7. The lowest R_{rs} measured *in situ* between 2000 and 2012 in Lake Taihu in different seasons.

References

Arnone RA, Wood M, Gould Jr RW. The evolution of optical water mass classification. Oceanography 2004;17(2).
Austin R. Inherent spectral radiance signatures of the ocean surface. Ocean color anal 1974;7410:1–20.
Bai Y, He XQ, Pan DL, Zhu QK, Gong F. The black water around the Changjiang (Yangtze) Estuary in the spring of 2003. Acta Oceanol Sin 2009;28:23–31.
Barber LB, Leenheer JA, Noyes TI, Stiles EA. Nature and transformation of dissolved organic matter in treatment wetlands. Environ Sci Technol 2001;35:4805–16.
Battin TJ. Dissolved organic matter and its optical properties in a blackwater tributary of the upper Orinoco river, Venezuela. Org Geochem 1998;28:561–9.
Berthon JF, Zibordi G. Optically black waters in the northern Baltic Sea. Geophys Res Lett 2010;37.
Bricaud A, Claustre H, Ras J, Oubelkheir K. Natural variability of phytoplanktonic absorption in oceanic waters: influence of the size structure of algal populations. Journal of Geophysical Research-Oceans 2004;109.
Bricaud A, Morel A, Prieur L. Absorption by dissolved organic matter of the sea (yellow substance) in the UV and visible domains. Limnol Oceanogr 1981;26:43–53.
Chen ZQ, Li Y, Pan JM. Distributions of colored dissolved organic matter and dissolved organic carbon in the Pearl River Estuary, China. Cont Shelf Res 2004;24:1845–56.
Chimney MJ, Pietro KC. Decomposition of macrophyte litter in a subtropical constructed wetland in south Florida (USA). Ecol Eng 2006;27:301–21.
Clark CD, Litz LP, Grant SB. Salt marshes as a source of chromophoric dissolved organic matter (CDOM) to Southern California coastal waters. Limnol Oceanogr 2008: 1923–33.
Clark DK. Phytoplankton pigment algorithms for the Nimbus-7 CZCS (Coastal Zone Color Scanner). Oceanography 1981:227–37. [from space].
Davis III SE, Corronado-Molina C, Childers DL, Day Jr JW. Temporally dependent C, N, and P dynamics associated with the decay of *Rhizophora mangle* L. leaf litter in oligotrophic mangrove wetlands of the Southern Everglades. Aquat Bot 2003;75:199–215.
Diaz RJ, Rosenberg R. Spreading dead zones and consequences for marine ecosystems. Science 2008;321:926–9.
Dierssen HM, Kudela RM, Ryan JP, Zimmerman RC. Red and black tides: quantitative analysis of water-leaving radiance and perceived color for phytoplankton, colored dissolved organic matter, and suspended sediments. Limnol Oceanogr 2006;51: 2646–59.
Duan H, Ma R, Hu C. Evaluation of remote sensing algorithms for cyanobacterial pigment retrievals during spring bloom formation in several lakes of East China. Remote Sens Environ 2012;126:126–35.
Duan HT, Ma RH, Xu XF, Kong FX, Zhang SX, Kong WJ, et al. Two-decade reconstruction of algal blooms in China's Lake Taihu. Environ Sci Technol 2009;43:3522–8.
Duan HT, Ma RH, Zhang YZ, Loiselle SA, Xu JP, Zhao CL, et al. A new three-band algorithm for estimating chlorophyll concentrations in turbid inland lakes. Environ Res Lett 2010;5:044009.
Duval B, Ludlam SD. The black water chemocline of meromictic Lower Mystic Lake, Massachusetts, U.S.A. Int Rev Hydrobiol 2001;86:165–81.
Feng Z, Fan C, Huang W, Ding S. Microorganisms and typical organic matter responsible for lacustrine "black bloom". Sci Total Environ 2014;470–471:1–8.
Gordon HR, Morel AYRemote assessment of ocean color for interpretation of satellite visible imagery: A review, 4. American Geophysical Union; 1983.
Guo L. Doing battle with the green monster of Taihu Lake. Science 2007;317:1166.
He W, Shang J, Lu X, Fan C. Effects of sludge dredging on the prevention and control of algae-caused black bloom in Taihu Lake, China. J Environ Sci 2013;25:430–40.
Hu C, Lee Z, Ma R, Yu K, Li D, Shang S. Moderate Resolution Imaging Spectroradiometer (MODIS) observations of cyanobacteria blooms in Taihu Lake, China. J Geophys Res Oceans 2010;115:C04002.
Hu CM, Muller-Karger FE, Vargo GA, Neely MB, Johns E. Linkages between coastal runoff and the Florida Keys ecosystem: a study of a dark plume event. Geophys Res Lett 2004;31.
IOCCG. Remote sensing of ocean colour in coastal, and other optically-complex, waters. In: Stuart V, editor. Reports of the International Ocean Colour Coordinating Group; 2000.
IOCCG. Remote sensing of inherent optical properties: fundamentals, tests of algorithms, and applications. In: Stuart V, editor. Reports of the International Ocean Colour Coordinating Group. 5. International Ocean-Colour Coordinating Group; 2006.
IOCCG. Why ocean colour? The societal benefits of ocean-colour radiometry. In: Stuart V, editor. Reports of the International Ocean Colour Coordinating Group; 2008.
Jansson M, Blomqvist P, Jonsson A, Bergstrom AK. Nutrient limitation of bacterioplankton, autotrophic and mixotrophic phytoplankton, and heterotrophic nanoflagellates in Lake Ortrasket. Limnol Oceanogr 1996;41:1552–9.
Jiang G, Ma R, Loiselle SA, Duan H. Optical approaches to examining the dynamics of dissolved organic carbon in optically complex inland waters. Environ Res Lett 2012; 7:034014.
Le C, Hu C, English D, Cannizzaro J, Chen Z, Kovach C, et al. Inherent and apparent optical properties of the complex estuarine waters of Tampa Bay: what controls light? Estuarine Coast Shelf Sci 2013;117:54–69.
Lee ZP, Carder KL, Arnone RA. Deriving inherent optical properties from water color: a multiband quasi-analytical algorithm for optically deep waters. Appl Opt 2002;41:5755–72.
Loisel H, Morel A. Non-isotropy of the upward radiance field in typical coastal (Case 2) waters. Int J Remote Sens 2001;22:275–95.
Loiselle S, Vione D, Minero C, Maurino V, Tognazzi A, Dattilo AM, et al. Chemical and optical phototransformation of dissolved organic matter. Water Res 2012;46:3197–207.
Loiselle SA, Bracchini L, Dattilo AM, Ricci M, Tognazzi A, Cozar A, et al. Optical characterization of chromophoric dissolved organic matter using wavelength distribution of absorption spectral slopes. Limnol Oceanogr 2009;54:590–7.

Losee RF, Wetzel RG. Littoral flow-rates within and around submersed macrophyte communities. Freshw Biol 1993;29:7–17.
Lu G, Ma Q. Monitoring and analysis on "black water aggregation" in Lake Taihu, 2009. J Lake Sci 2010;22:481–7.
Ma R, Tang J, Dai J. Bio-optical model with optimal parameter suitable for Taihu Lake in water colour remote sensing. Int J Remote Sens 2006;27:4305–28.
Ma RH, Pan DL, Duan HT, Song QJ. Absorption and scattering properties of water body in Taihu Lake, China: backscattering. Int J Remote Sens 2009;30:2321–35.
Madsen JD, Chambers PA, James WF, Koch EW, Westlake DF. The interaction between water movement, sediment dynamics and submersed macrophytes. Hydrobiologia 2001;444:71–84.
Maffione RA, Dana DR. Instruments and methods for measuring the backward-scattering coefficient of ocean waters. Appl Opt 1997;36:6057–67.
McCollough C. Color adaptation of edge-detectors in the human visual system. Science 1965;149:1115–6.
Mitchell BG. Algorithms for determining the absorption coefficient for aquatic particulates using the quantitative filter technique. Proc SPIE 1990;1302:137.
Morel A. Optical modeling of the upper ocean in relation to its biogenous matter content (case-I waters). J Geophys Res Oceans 1988;93:10749–68.
Morel A, Gentili B. Diffuse-reflectance of oceanic waters. 2. Bidirectional aspects. Appl Opt 1993;32:6864–79.
Morel A, Gentili B. A simple band ratio technique to quantify the colored dissolved and detrital organic material from ocean color remotely sensed data. Remote Sens Environ 2009;113:998–1011.
Mostofa KMG, Yoshioka T, Mottaleb A, Vione D. Photobiogeochemistry of organic matter. Springer; 2013.
Mueller JL, Fargion GS. Ocean optics protocols for satellite ocean color sensor validation. Revision 2003;6.
Naik P, D'Sa EJ, HdR Gomes, Goés JI, Mouw CB. Light absorption properties of southeastern Bering Sea waters: analysis, parameterization and implications for remote sensing. Remote Sens Environ 2013;134:120–34.
O'Donnell DM, Effler SW, Strait CM, Leshkevich GA. Optical characterizations and pursuit of optical closure for the western basin of Lake Erie through in situ measurements. J Great Lakes Res 2010;36:736–46.
Pascoal C, Cassio F. Contribution of fungi and bacteria to leaf litter decomposition in a polluted river. Appl Environ Microbiol 2004;70:5266–73.
Pedersen MF, Borum J. Nutrient control of algal growth in estuarine waters. Nutrient limitation and the importance of nitrogen requirements and nitrogen storage among phytoplankton and species of macroalgae, 142. Oldendorf: Marine Ecology Progress Series; 1996. p. 261–72.
Pucciarelli S, Buonanno F, Pellegrini G, Pozzi S, Ballarini P, Miceli C. Biomonitoring of Lake Garda: identification of ciliate species and symbiotic algae responsible for the "black-spot" bloom during the summer of 2004. Environ Res 2008;107:194–200.
Qin BQ, Xu PZ, Wu QL, Luo LC, Zhang YL. Environmental issues of Lake Taihu, China. Hydrobiologia 2007;581:3–14.
Sathyendranath S, Cota G, Stuart V, Maass H, Platt T. Remote sensing of phytoplankton pigments: a comparison of empirical and theoretical approaches. Int J Remote Sens 2001;22:249–73.
Sayer CD, Davidson TA, Jones JI. Seasonal dynamics of macrophytes and phytoplankton in shallow lakes: a eutrophication-driven pathway from plants to plankton? Freshw Biol 2010;55:500–13.
Shanmugam P. New models for retrieving and partitioning the colored dissolved organic matter in the global ocean: implications for remote sensing. Remote Sens Environ 2011;115:1501–21.
Shen Q, Zhou Q, Shang J, Shao S, Zhang L, Fan C. Beyond hypoxia: occurrence and characteristics of black blooms due to the decomposition of the submerged plant *Potamogeton crispus* in a shallow lake. J Environ Sci 2014;26:281–8.
Squires MM, Lesack LFW, Huebert D. The influence of water transparency on the distribution and abundance of macrophytes among lakes of the Mackenzie Delta, Western Canadian Arctic. Freshw Biol 2002;47:2123–35.
Stabenau ER, Zepp RG, Bartels E, Zika RG. Role of the seagrass *Thalassia testudinum* as a source of chromophoric dissolved organic matter in coastal south Florida. Mar Ecol Prog Ser 2004;282:59–72.
Stahl JB. Black water and two peculiar types of stratification in an organically loaded strip-mine lake. Water Res 1979;13:467–71.
Strickland J, Parsons TA practical handbook of seawater analysis, 167. Canada: Fisheries Research Board; 1972. p. 310.
Sugiura N, Nakano K. Causative microorganisms for musty odor occurrence in the eutrophic Lake Kasumigaura. Hydrobiologia 2000;434:145–50.
Twilley R, Kemp W, Staver K, Stevenson JC, Boynton W. Nutrient enrichment of estuarine submersed vascular plant communities. 1. Algal growth and effects on production of plants and associated communities, 23. Oldendorf: Marine ecology progress series; 1985. p. 179–91.
Tzortziou M, Neale PJ, Osburn CL, Megonigal JP, Maie N, Jaffe R. Tidal marshes as a source of optically and chemically distinctive colored dissolved organic matter in the Chesapeake Bay. Limnol Oceanogr 2008;53:148–59.
Tzortziou M, Subramaniam A, Herman JR, Gallegos CL, Neale PJ, Harding LW. Remote sensing reflectance and inherent optical properties in the mid Chesapeake Bay. Estuar Coast Shelf Sci 2007;72:16–32.
Valiela I, Teal JM, Allen SD, Van Etten R, Goehringer D, Volkmann S. Decomposition in salt marsh ecosystems: the phases and major factors affecting disappearance of above-ground organic matter. J Exp Mar Biol Ecol 1985;89:29–54.
Wang XC, Litz L, Chen RF, Huang W, Feng P, Altabet MA. Release of dissolved organic matter during oxic and anoxic decomposition of salt marsh cordgrass. Mar Chem 2007;105:309–21.
Watanabe S, Laurion I, Chokmani K, Pienitz R, Vincent WF. Optical diversity of thaw ponds in discontinuous permafrost: a model system for water color analysis. J Geophys Res 2011;116:G02003.
Wu G, Cui L, Duan H, Fei T, Liu Y. Absorption and backscattering coefficients and their relations to water constituents of Poyang Lake. China Appl Opt 2011;50:6358–68.
Xiang J, Pang Y, Li Y, Wei H, Wang P, Liu X. Hydrostatic settling suspended matter of large shallow lake. Adv Water Sci 2008;19:111.
Yang M, Yu JW, Li ZL, Guo ZH, Burch M, Lin TF. Taihu Lake not to blame for Wuxi's woes. Science 2008;319:158-158.
Yentsch CS. Measurement of visible light absorption by particulate matter in the ocean. Limnol Oceanogr 1962:207–17.
Zhang YL, van Dijk MA, Liu ML, Zhu GW, Qin BQ. The contribution of phytoplankton degradation to chromophoric dissolved organic matter (CDOM) in eutrophic shallow lakes: field and experimental evidence. Water Res 2009;43:4685–97.
Zhao J, Hu C, Lapointe B, Melo N, Johns E, Smith R. Satellite-observed black water events off Southwest Florida: implications for coral reef health in the Florida Keys National Marine Sanctuary. Remote Sens 2013;5:415–31.